The Astrophysical Journal Letters, 870:L15 (5pp), 2019 January 10 https://doi.org/10.3847/2041-8213/aaf96b

The Optical Afterglow of GW170817 at One Year Post-merger

G. P. Lamb[1], J. D. Lyman[2], A. J. Levan[2], N. R. Tanvir[1], T. Kangas[3], A. S. Fruchter[3], B. Gompertz[2], J. Hjorth[4], I. Mandel[5,6], S. R. Oates[2], D. Steeghs[2], and K. Wiersema[2]
[1] Department of Physics and Astronomy, University of Leicester, LE1 7RH, UK; gpl6@leicester.ac.uk
[2] Department of Physics, University of Warwick, Coventry, CV4 7AL, UK
[3] Space Telescope Science Institute, 3700 San Martin Drive, Baltimore, MD 21218, USA
[4] DARK, Niels Bohr Institute, University of Copenhagen, Lyngbyvej 2, Copenhagen DK-2100, Denmark
[5] Institute for Gravitational Wave Astronomy, School of Physics and Astronomy, University of Birmingham, Birmingham, B15 2TT, UK
[6] Monash Centre for Astrophysics, School of Physics and Astronomy, Monash University, Clayton, Victoria 3800, Australia
Received 2018 November 28; revised 2018 December 13; accepted 2018 December 18; published 2019 January 9

Abstract

We present observations of the optical afterglow of GRB 170817A, made by the *Hubble Space Telescope*, between 2018 February and August, up to one year after the neutron star merger GW170817. The afterglow shows a rapid decline beyond 170 days, and confirms the jet origin for the observed outflow, in contrast to more slowly declining expectations for "failed-jet" scenarios. We show here that the broadband (radio, optical, X-ray) afterglow is consistent with a structured outflow where an ultra-relativistic jet, with a Lorentz factor of $\Gamma \gtrsim 100$, forms a narrow core ($\sim 5^\circ$) and is surrounded by a wider angular component that extends to $\sim 15^\circ$, which is itself relativistic ($\Gamma \gtrsim 5$). For a two-component model of this structure, the late-time optical decline, where $F \propto t^{-\alpha}$, is $\alpha = 2.20 \pm 0.18$, and for a Gaussian structure the decline is $\alpha = 2.45 \pm 0.23$. We find the Gaussian model to be consistent with both the early ~ 10 days and late $\gtrsim 290$ days data. The agreement of the optical light curve with the evolution of the broadband spectral energy distribution, and its continued decline, indicates that the optical flux is arising primarily from the afterglow and not any underlying host system. This provides the deepest limits on any host stellar cluster with a luminosity $\lesssim 4000\, L_\odot$ ($M_{\rm F606W} \gtrsim -4.3$).

Key words: gravitational waves – relativistic processes – stars: neutron

1. Introduction

The first binary neutron star merger detected via gravitational waves (GW170817) was accompanied by a weak short-duration gamma-ray burst (GRB 170817A Abbott et al. 2017a), a radioactively powered kilonova, and a long-lived afterglow (e.g., Abbott et al. 2017b). The steady rise of the afterglow from a ~ 10 days post-merger, which was traced at radio, X-ray, and optical wavelengths (e.g., Hallinan et al. 2017; Margutti et al. 2017, 2018; Troja et al. 2017, 2018; Alexander et al. 2018; D'Avanzo et al. 2018; Dobie et al. 2018; Lyman et al. 2018; Mooley et al. 2018c, 2018a, 2018b; Nynka et al. 2018; Resmi et al. 2018; van Eerten et al. 2018; Piro et al. 2019), distinguished GRB 170817A (alongside its intrinsic low-luminosity) from cosmological short gamma-ray bursts (GRBs). This called into question the link between GW170817 and the progenitors of other short GRBs.

Following a neutron star merger, a jet, launched due to the rapid accretion of ejected matter onto a compact remnant, will propagate through the merger ejecta medium. The interaction of the jet with the ejecta will result in a structured outflow where the wider components are the product of a cocoon of accelerated ejecta material (e.g., Nagakura et al. 2014; Murguia-Berthier et al. 2017). The profile of this outflow depends on the mass and density of the ejected material and the initial structure of the jet. Simulations of jet propagation through the merger ejecta can result in outflows that have a Gaussian structure (Xie et al. 2018). This structure is responsible for driving the afterglow's evolution. More recent simulations are beginning to reveal the structure of the jet at launch (Kathirgamaraju et al. 2018). The afterglow to GRB 170817A is the first opportunity to convincingly probe the structure of these outflows.

For a favorably inclined gravitational-wave (GW) detected neutron star merger, the temporal behavior of the afterglow, viewed off the jet central axis, can probe the outflow structure and give an insight into the outflows that accompany cosmological short GRBs (Lamb & Kobayashi 2017; Lazzati et al. 2017a). The slow rise of the afterglow is indicative of an outflow with either an angular or radial structure.

In the angular model, the earliest afterglow observations are of the outflow components nearest to the line of sight. As the outflow decelerates and expands an increasing fraction of the outflow becomes visible. A slow rise to peak, as observed in the afterglow of GRB 170817A, can be recreated where the angular structure of the outflow consists of a fast and energetic core (the jet, with a Lorentz factor of $\Gamma \gtrsim 100$) and a slower, less energetic, wide component (a cocoon, $\Gamma \lesssim 10$; e.g., Lazzati et al. 2018).

In the radial model the outflow is wide and has a stratified velocity profile. The fastest components ($\Gamma \sim 10$) decelerate first and the resultant blast wave is refreshed by slower components as they catch up to the shock front. The total energy of the blast wave increases until the slowest component peaks; the dynamics of the final decelerating blast wave are determined by the slowest component ($\Gamma \sim 1.4$–2.0). The afterglow rise following GRB 170817A can be recreated by a wide-angled outflow with such a radial profile (e.g., Kasliwal et al. 2017).

At ~ 150 days post-merger, the X-ray (D'Avanzo et al. 2018; Margutti et al. 2018) and radio (Dobie et al. 2018) frequency light curves peaked and began to decline. Distinctive behavior for the decline rate of the afterglow is expected depending on the dynamical and structural nature of the outflow; a steeper decline is expected for the initially ultra-relativistic angular structured jet scenario (Lamb et al. 2018; Troja et al. 2018). A

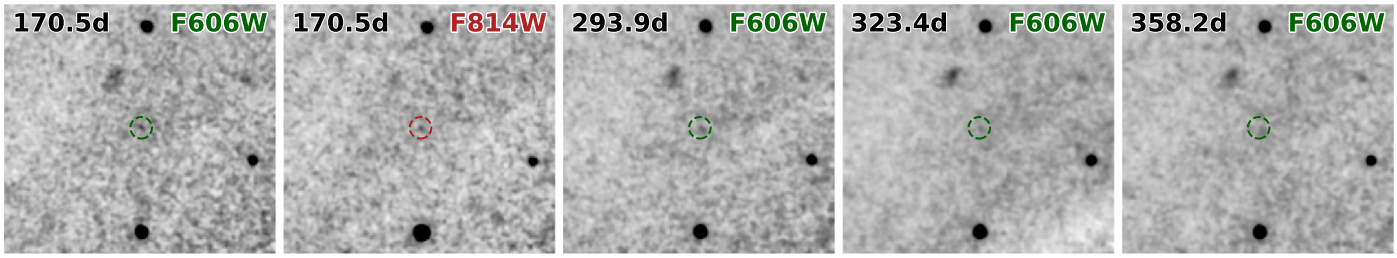

Figure 1. Very late-time *HST* imaging of GW170817. Images are 5 arcsec per side and the filter and rest-frame days since GW170817 are indicated in each sub-figure. An isophotal elliptical model of the smooth galaxy light has been subtracted from each figure (see the text) and the images have been Gaussian-smoothed to aid the eye. Dashed circles, centered on the location of GW170817, from alignment with earlier *HST* epochs, are 0.″25 radius. North is up and east is left.

Table 1
GW170817 *HST* WFC3 Photometry

Date	MJD[a] (day)	Time Since Merger (day)	Tot. Exp. Time s	Filter	AB Mag.
2018 Feb 5	58154.65	170.5	2400	F814W	26.31 ± 0.15
	58154.72	170.5	2400	F606W	27.16[b] ± 0.17
2018 Jun 10	58279.27	293.9	5220	F606W	27.75 ± 0.20
2018 Jul 10	58309.14	323.4	14070	F606W	28.05 ± 0.17
2018 Aug 14	58344.23	358.2	14070	F606W	28.78 ± 0.39

Notes. Magnitudes have been corrected for foreground Galactic extinction following Schlafly & Finkbeiner (2011).
[a] At start of exposures.
[b] Appears spurious considering contemporaneous data, see the text.

steep decline, confirming the presence of a strong jet and ruling out the wide cocoon of the radial model, was revealed by recent radio afterglow observations (Mooley et al. 2018b). The presence of an energetic jet within the outflow was additionally supported by the results from the very long baseline interferometry (VLBI) of the radio source. The superluminal motion of the source was observed, revealing the relativistic motion of a narrow jet core launched during the merger (Ghirlanda et al. 2018; Mooley et al. 2018a).

In this Letter we present the optical light curve of the afterglow of GRB 170817A from *Hubble Space Telescope* (*HST*) imaging covering one year post-merger. The photometry is presented in Section 2. We supplement these data with radio and X-ray frequency observations to investigate the behavior of the declining afterglow within the structured jet scenario. In Section 3 we fit a simple two-component jet-cocoon structure and a Gaussian structure that are both consistent with the observed data. The Gaussian-structured outflow gives a steeper decline post-peak and is more consistent with the very late-time observations at optical and radio frequencies. The discussion and conclusions are given in Sections 4 and 5, respectively.

2. Additional *HST* Photometry

Our *HST* observations were carried out in programs GO14771 (PI: Tanvir) and GO15482 (PI: Lyman) using WFC3 in filters F606W and F814W. Early *HST* photometry of the kilonova was presented in Tanvir et al. (2017). Here we concentrate on later observations when the afterglow is dominant, extending up to one year after the merger. The first epoch of these data were presented in Lyman et al. (2018), and here we present four additional epochs of observations, the results of which are shown in Table 1 and Figure 1. Non-detections in the near-infrared observations from 2017 December caused us to focus on optical bands for the subsequent epochs in 2018 February, June, July, and August, corresponding to ∼171, 294, 323, and 358 days post-merger, respectively. Observations employed dithered exposures within visits in order to improve upon the native pixel scale using ASTRODRIZZLE within DRIZZLEPAC. In addition, as the July and August epochs' exposures were split across multiple visits, TWEAKREG was employed to achieve accurate alignment between the visits (rms ∼0.10–0.15 pixel). Further details of the reduction and analysis are presented in Lyman et al. (2018).

Our photometry was performed on the drizzled images after subtracting the smooth galaxy light through isophotal ellipse fitting with the IRAF task ELLIPSE. A 0.″08 aperture was used and corrected using provided encircled energy tables.[7] Our optical light curve mimics the behavior seen at other frequencies by peaking somewhere between our 110 and 171 days epochs, before steeply declining.

For the February epoch, our photometry indicated a significant and unexpected change in the color of the afterglow compared to our 2017 December observations. Although the F814W flux remained almost constant, a drop (at the ∼3–4σ level) of ∼0.75 mag was seen in our F606W measurement. Inspection of the individual frames did not reveal any obvious detector artifacts. We note that a near-contemporaneous measurement in F606W was made by Piro et al. (2019), and, although a low significance detection at 26.4 ± 0.4 mag, this suggests no significant change of flux with respect to 2017 December. Given the achromatic evolution of the synchrotron emission, we would not expect such a large color change, particularly over neighboring filters. Coupled with no change in the broad band evolution (i.e., radio or X-rays), we suggest that these observations are most likely a statistical fluke rather than any real color evolution in the afterglow.

Our August epoch has a marginal detection of flux and we cannot say for certain if this is entirely down to the afterglow

[7] http://www.stsci.edu/hst/wfc3/analysis/uvis_ee

itself, or whether some underlying surface brightness fluctuation in the galaxy light or cluster system is contributing, or at what level (indeed the source becomes visually ambiguous at this epoch; see Figure 1). The measurement does however allow us to place deep constraints on any underlying host cluster, which could not be significantly brighter than the flux level we see. At a distance modulus of $\mu = 33.05 \pm 0.18$ mag (Hjorth et al. 2017; Cantiello et al. 2018) this translates to a limit of $M_{F606W} = -4.3 \pm 0.4$ mag ($\sim 4000 L_{\odot}$), fainter than $\sim$99% of global clusters (GCs) found in the Local Group (Harris 1996, 2010 edition; see method of Lyman et al. 2014). Further, as shown later, our June epoch (294 days post-merger) is almost contemporaneous with radio and X-ray measurements and our photometry for this epoch agrees well with the broadband spectral energy distribution (SED) of the afterglow. However, when subtracting the August image from our June epoch and repeating the photometry on this subtracted image, we found the resultant flux was significantly below this SED-inferred level. This would suggest that the flux is dominated by the transient, rather than any underlying fluctuation, at least at this epoch. The continued decline of the optical flux up to the limit of our observations also indicates that the transient is the source of the flux, rather than any underlying persistent source.

3. Afterglow Modeling

The afterglow flux of GRB 170817A exhibits a slow rise to peak from $\sim$10 to 150 days as $\sim t^{0.8}$. This behavior is best explained by the angular structure of the outflow. The wide angle components of a structured outflow are likely to be a cocoon of merger ejecta material that has been shocked and accelerated by the passage of an ultra-relativistic jet, where the jet is at the core of the outflow.

Post-peak, the rapid decline with an index of $\alpha > 1.5$, where the flux $F \propto t^{-\alpha}$, indicates that the light curve at late times is dominated by an initially ultra-relativistic velocity jet or the core of the outflow (Lamb et al. 2018). A rapid post-peak decline has been confirmed by X-ray and radio observations (Alexander et al. 2018; Mooley et al. 2018b; Nynka et al. 2018; van Eerten et al. 2018) and here via optical observations with *HST*.

We determine light curves for two angular structured outflow models that give good fits to the data. Motivated by the VLBI observations of a superluminal core with a half-opening angle, $\theta_c \lesssim 5°$, and observed at an inclination from the outflow central axis, $\iota \sim 20°$ (Mooley et al. 2018a), we limit the range for these two parameters in our model fits to $0.6° \leqslant \theta_c \leqslant 6°$ and the inclination to $17° \leqslant \iota \leqslant 23°$. With these tight constraints we consider the following models.

1. Model (A): a simple two-component structure consisting of a narrow uniform $<\theta_c$, energetic, and ultra-relativistic $\Gamma \gtrsim 100$ core surrounded by a wide, relativistic cocoon of $\Gamma = 5$ with 10% of the core energy per steradian over angles $\theta_c - \theta_j$, where $\theta_j = 15°$ and is the edge of the outflow.[8]
2. Model (B): a Gaussian structure where the energy per steradian is $\propto e^{-\theta^2/\theta_c^2}$ and the Lorentz factor is $\propto e^{-\theta^2/2\theta_c^2}$ (and condition $\Gamma > 1$) within θ_j.

Model (A) is a simple structure based on Lazzati et al. (2017a, 2017b) and Lamb & Kobayashi (2017), where the Lorentz factor of the cocoon is $\Gamma < 10$. The fixed parameters ensure that the cocoon is energetic enough to contribute at early times and reduces the number of parameters in the fit. Model (B) was used originally in relation to the GRB 170817A afterglow by Resmi et al. (2018) and Lamb & Kobayashi (2018). We limit the opening angle of the outflow to $\sim$15°. For Model (A), a much wider cocoon would require a more complex structure, and for Model (B), the low energetics of wider components would contribute insignificantly to the light curve.

The afterglow flux from each model is calculated using an updated version of the structured outflow method described in Lamb & Kobayashi (2017) and Lyman et al. (2018). The dynamics for the expanding blast wave follow the analytic solution in Pe'er (2012) and includes sideways expansion at the sound speed[9] as well as a more accurate synchrotron flux estimation (see Lamb et al. 2018).

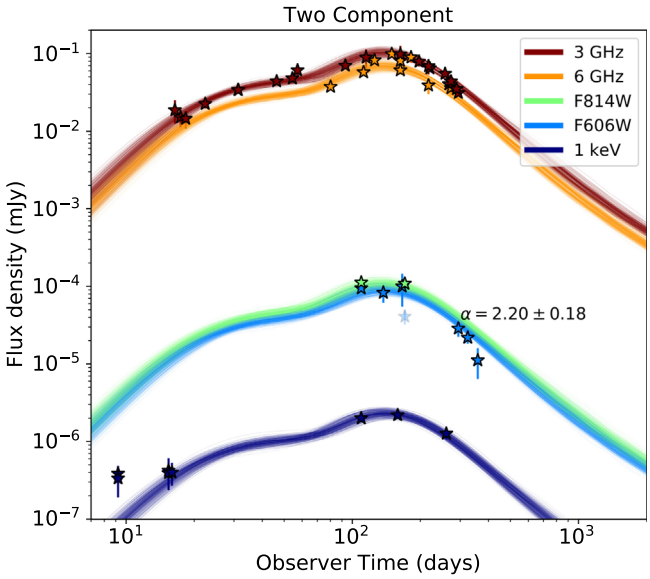

Figure 2. Model light curves for 400 randomly selected parameter sets from an MCMC for Model (A). The stars represent the data points and the error bars are 1σ (error bars may be hidden by the markers). Light curves at 3 GHz, 6 GHz, 3.8×10^{14} Hz (F814W), 5.1×10^{14} Hz (F606W), and 1 keV are shown. The decline index α between 260 and 300 days is annotated. The faint point at $\sim$170 days shows the anomalous F606W point discussed in Section 2.

Table 2
Inferred Afterglow Parameters

Parameter	Prior Range	Model (A)	Model (B)	Unit
$\log_{10} E_{\rm iso,c}$	50–53	$52.0^{+0.6}_{-0.9}$	$52.4^{+0.4}_{-0.5}$	$\log_{10}$ erg
$\Gamma_{0,c}$	10–1000	88^{+40}_{-28}	666^{+231}_{-272}	⋯
θ_c	0.01–0.1	$0.07^{+0.01}_{-0.01}$	$0.09^{+0.01}_{-0.01}$	rad
ι	0.3–0.4	$0.36^{+0.03}_{-0.03}$	$0.34^{+0.02}_{-0.02}$	rad
$\log_{10} \varepsilon_B$	−4–0.5	$-2.4^{+1.4}_{-0.9}$	$-2.1^{+0.8}_{-1.0}$	⋯
$\log_{10} \varepsilon_e$	−4–0.5	$-1.3^{+0.6}_{-0.7}$	$-1.4^{+0.5}_{-0.6}$	⋯
$\log_{10} n_0$	−5–0	$-3.3^{+0.6}_{-1.0}$	$-4.1^{+0.5}_{-0.5}$	$\log_{10}$ cm^{-3}
p	2.01–2.25	$2.17^{+0.01}_{-0.01}$	$2.16^{+0.01}_{-0.01}$	⋯

Note. Subscript "c" indicates the jet central point. Parameter values are the median from EMCEE distributions, uncertainties represent the 16th and 84th percentiles.

[8] A energetic cocoon that can account for the afterglow light curve of $t \lesssim 80$ days and with an initial Lorentz factor of $\Gamma < 5$ will dominate the late-time decline resulting in a decay index of $\alpha \lesssim 2.0$ (Lamb et al. 2018). Such a decline is ruled out by the data.

[9] Sideways expansion of the outflow is required at late times as the decline is $\alpha \gtrsim 1.6$, the limit expected for a jetted outflow with these parameters. Using a more realistic expansion (e.g., van Eerten & MacFadyen 2012) will have only a small effect on the fitted parameters.

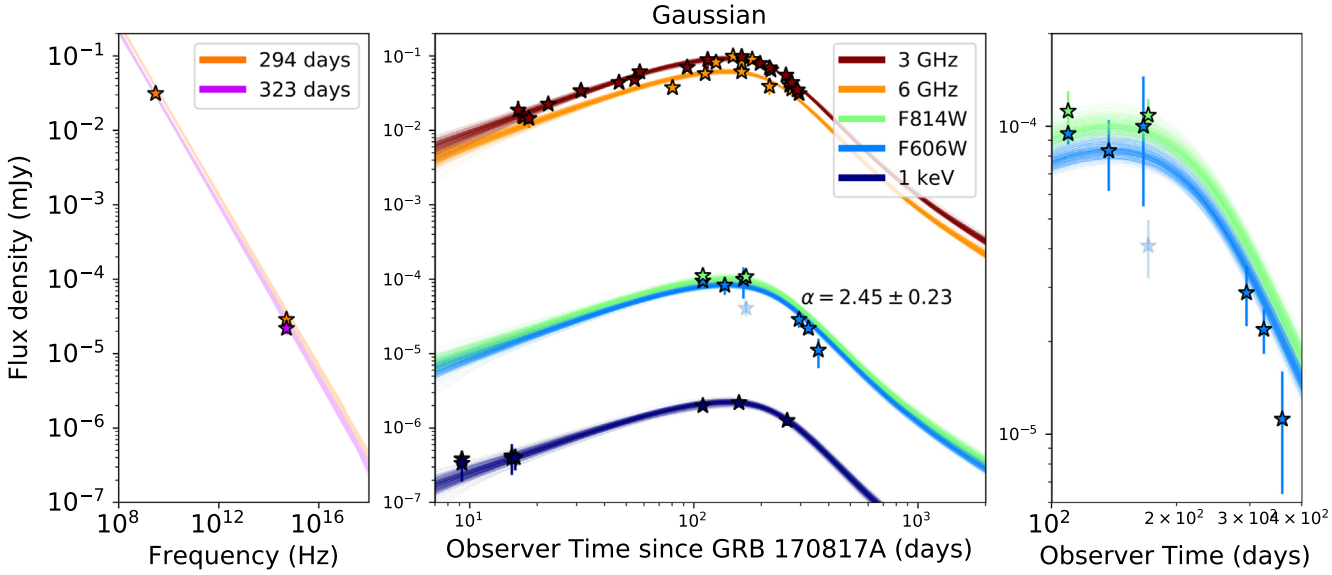

Figure 3. Left panel: 400 SEDs at 294 days (red line) and 323 days (purple line). The stars show data for each epoch and the error bars are smaller than the marker size. Middle panel: model light curves for 400 randomly selected parameter sets from an MCMC for Model (B). Data are the same as those in Figure 2. The decline index α between 260 and 300 days is annotated. Right panel: zoom-in of the optical data and light curves between 100 and 400 days post GRB 170817A/GW170817.

We use a Markov Chain Monte Carlo (MCMC) EMCEE to determine the best parameter fits for each model using the flux at 3 and 6 GHz (Dobie et al. 2018; Margutti et al. 2018; Mooley et al. 2018c, 2018b), the *HST* optical data points (this study; Lyman et al. 2018; Piro et al. 2019), and *Chandra* X-ray flux at 1 keV (Margutti et al. 2017; Troja et al. 2017, 2018). For each model we fit eight parameters,

$$\Phi = [\, E_{\rm iso,c},\ \Gamma_{0,c},\ \theta_c,\ \iota,\ \varepsilon_B,\ \varepsilon_e,\ n_0,\ p\,],$$

where $E_{\rm iso,c}$ is the isotropic equivalent energy of the central core point, $\Gamma_{0,c}$ is the bulk Lorentz factor pre-deceleration of the central core point, ε_B and ε_e are the microphysical parameters, n_0 is the ambient medium particle density, and p the accelerated electron power-law index.[10]

The parameter constraints for each model are shown in Table 2 where the uncertainties represent the 16th and 84th percentiles. We see the expected correlations and degeneracies within the parameter distributions, i.e., ε_B with n and both ε_B and n with the core energy. Model (A) favors an inclination toward the upper limit within our range and ε_e is pushed against the upper bound, whereas for Model (B) we see a positive correlation between core angle and inclination and find that the core energy, Lorentz factor, and jet core angle favor the upper half of the parameter range.

For each model we show 400 light curves using randomly selected parameters drawn from the sample. The light curves for Model (A) are shown in Figure 2 and the light curves for Model (B) are shown in Figure 3. The light curve at 3 GHz, 3.8×10^{14} Hz (F814W), 5.1×10^{14} Hz (F606W), and 1 keV are shown with data as stars. The temporal decline, α, calculated between 260 and 300 days at optical frequencies, is $\alpha = 2.20 \pm 0.18$ for Model (A) and $\alpha = 2.45 \pm 0.23$ for Model (B). The optical data, the Model (B) light curve, and the model SED at 294 and 323 days are highlighted in Figure 3.

[10] Parameters $E_{\rm iso,c}$, ε_B, ε_e, and n_0 have logarithmic flat priors, while $\Gamma_{0,c}$, θ_c, ι, and p have flat priors. We use 40 walkers, 2000 burn-in steps and 15,000 steps per model.

4. Discussion

We have presented optical observations made by *HST* of the afterglow to GRB 170817A between 2018 February and August (see Table 1). Using this data we confirm the rapid decline of the afterglow indicative of an initially ultra-relativistic jet viewed off-axis. Combining the optical data with radio wavelength observations at 3 and 6 GHz, and X-ray frequency data at 1 keV, we use EMCEE to fit two outflow structure models (see Figures 2 and 3).

The post-peak decline seen here at optical frequencies, and at radio frequencies by Mooley et al. (2018b), is rapid; the decline index is $\alpha \gtrsim 2.1$. An $\alpha \sim p$ is expected for an on-axis observed afterglow following the jet-break, a steeper decline is expected for an observer outside of the initial jet half-opening angle (e.g., van Eerten et al. 2012), and the latest data points indicate a very rapid decline at late times. Such a rapid decline requires an initially ultra-relativistic and collimated outflow—a jet—and rules out the possibility here of a wide-angled mildly relativistic outflow (Lamb et al. 2018).

The two outflow models used to fit the afterglow data show differing late-time declines. The two-component Model(A) shows a shallower decline at $\alpha \sim 2.2$, and the Gaussian-structured outflow Model(B) shows a steeper decline at $\alpha \sim 2.5$, between 260 and 300 days post-merger. If the decline is shown to steepen at later epochs then the expansion description or the jet core structure should be reconsidered.

The origin of the gamma-ray emission in GRB 170817A is debated. A faint GRB would be an expectation for an off-axis observation. However, the spectral peak energy for the prompt emission and the lack of an early afterglow challenges the simple off-axis model (e.g., Ioka & Nakamura 2018; Lamb & Kobayashi 2018; Matsumoto et al. 2019; Nakar et al. 2018). The leading explanations for the prompt origin include a short GRB seen off-axis, but considering more complex emission models (e.g., Eichler 2018; Zhang et al. 2018), a GRB scattered by cocoon material (Kisaka et al. 2018), and a burst of gamma-rays as a result of a cocoon shock breakout (Gottlieb et al. 2018). It is beyond the scope of this work to determine the

origin of the prompt emission, although the steep sides of the core in both models (A) and (B) are consistent with the description Kisaka et al. (2018) required for scattered prompt emission.

We have tested only angular structure models and this is supported by the success of Model(A) at reproducing the early afterglow data. Where the Lorentz factor of the cocoon is <5, the late-time afterglow decline is shallower than $\alpha \lesssim 2$ due to the contribution of the cocoon. This supports the need for a relativistic outflow from core to edge. We note that the Gaussian structure can account for all of the data from 10 days, whereas the two-component model fails to recreate the first X-ray frequency data points (see Figure 2).

Both models have a peak of ∼140–160 days and predict a rapid decline $\alpha \gtrsim 2.0$. The transition to a Newtonian blast wave is seen more prominently in the Gaussian model at ∼700 days post-merger, although this is below the detection threshold at all frequencies. The counter jet will contribute to the light curve beyond the range of the figures at $\sim 10^4$ days.

5. Conclusions

Hubble Space Telescope observations of the afterglow of GRB 170817A, taken from 171 days to one year from merger GW170817, show it to be rapidly declining in flux. We find the declining optical flux is most consistent with arising from the afterglow, matching the behavior seen at other frequencies, and thus can be used to place the most stringent constraints on any underlying globular cluster system, which must be $M_{\rm F606W} \gtrsim -4.3 \pm 0.4$ mag.

We have modeled the afterglow using both a two-component jet model, consisting of a narrow highly relativistic core and a wider-angle component, and a Gaussian-structured outflow. Both scenarios are able to broadly recreate the steep decline post-peak. Such a steep decline requires an initially collimated, highly relativistic outflow and confirms that a successful jet was launched in GRB 170817A, in agreement with other lines of evidence (Ghirlanda et al. 2018; Mooley et al. 2018a). We find most consistency with the Gaussian outflow to describe our very late-time photometry (although uncertainties in the measurements are large for these epochs).

Based on observations made with the NASA/ESA *Hubble Space Telescope*, obtained from the data archive at the Space Telescope Science Institute (STScI). STScI is operated by the Association of Universities for Research in Astronomy, Inc. under NASA contract NAS 5-26555. These observations are associated with programs GO 15482 (J.D.L.) and GO 14771 (N.R.T.). G.P.L. is supported by STFC grant ST/N000757/1 and thanks Om Salafia for useful discussions. J.D.L. acknowledges support from STFC grant ST/P000495/1. A.J.L. acknowledges that this project received funding from the European Research Council (ERC) under the European Union's Horizon 2020 research and innovation program (grant agreement 725246). J.H. acknowledges support by a VILLUM FONDEN Investigator grant (project number 16599). S.R.O. acknowledges support of the Leverhulme Trust Early Career Fellowship. We thank the anonymous referee for the comments.

Facility: HST(WFC3).

Software: astropy (Astropy Collaboration et al. 2013), DrizzlePac STSCI Development Team (2012), emcee (Foreman-Mackey et al. 2013), SExtractor (Bertin & Arnouts 1996).

ORCID iDs

G. P. Lamb https://orcid.org/0000-0001-5169-4143
A. J. Levan https://orcid.org/0000-0001-7821-9369
N. R. Tanvir https://orcid.org/0000-0003-3274-6336
T. Kangas https://orcid.org/0000-0002-5477-0217
J. Hjorth https://orcid.org/0000-0002-4571-2306
I. Mandel https://orcid.org/0000-0002-6134-8946
K. Wiersema https://orcid.org/0000-0002-9133-7957

References

Abbott, B. P., Abbott, R., Abbott, T. D., et al. 2017a, ApJL, 848, L13
Abbott, B. P., Abbott, R., Abbott, T. D., et al. 2017b, ApJL, 848, L12
Alexander, K. D., Margutti, R., Blanchard, P. K., et al. 2018, ApJL, 863, L18
Astropy Collaboration, Robitaille, T. P., Tollerud, E. J., et al. 2013, A&A, 558, A33
Bertin, E., & Arnouts, S. 1996, A&AS, 117, 393
Cantiello, M., Jensen, J. B., Blakeslee, J. P., et al. 2018, ApJL, 854, L31
D'Avanzo, P., Campana, S., Salafia, O. S., et al. 2018, A&A, 613, L1
Dobie, D., Kaplan, D. L., Murphy, T., et al. 2018, ApJL, 858, L15
Eichler, D. 2018, ApJL, 869, L4
Foreman-Mackey, D., Hogg, D. W., Lang, D., & Goodman, J. 2013, PASP, 125, 306
Ghirlanda, G., Salafia, O. S., Paragi, Z., et al. 2018, arXiv:1808.00469
Gottlieb, O., Nakar, E., Piran, T., & Hotokezaka, K. 2018, MNRAS, 479, 588
Hallinan, G., Corsi, A., Mooley, K. P., et al. 2017, Sci, 358, 1579
Harris, W. E. 1996, AJ, 112, 1487
Hjorth, J., Levan, A. J., Tanvir, N. R., et al. 2017, ApJL, 848, L31
Ioka, K., & Nakamura, T. 2018, PTEP, 2018, 043E02
Kasliwal, M. M., Nakar, E., Singer, L. P., et al. 2017, Sci, 358, 1559
Kathirgamaraju, A., Tchekhovskoy, A., Giannios, D., & Barniol Duran, R. 2018, arXiv:1809.05099
Kisaka, S., Ioka, K., Kashiyama, K., & Nakamura, T. 2018, ApJ, 867, 39
Lamb, G. P., & Kobayashi, S. 2017, MNRAS, 472, 4953
Lamb, G. P., & Kobayashi, S. 2018, MNRAS, 478, 733
Lamb, G. P., Mandel, I., & Resmi, L. 2018, MNRAS, 481, 2581
Lazzati, D., Deich, A., Morsony, B. J., & Workman, J. C. 2017a, MNRAS, 471, 1652
Lazzati, D., López-Cámara, D., Cantiello, M., et al. 2017b, ApJL, 848, L6
Lazzati, D., Perna, R., Morsony, B. J., et al. 2018, PhRvL, 120, 241103
Lyman, J. D., Lamb, G. P., Levan, A. J., et al. 2018, NatAs, arXiv:1801.02669
Lyman, J. D., Levan, A. J., Church, R. P., Davies, M. B., & Tanvir, N. R. 2014, MNRAS, 444, 2157
Margutti, R., Alexander, K. D., Xie, X., et al. 2018, ApJL, 856, L18
Margutti, R., Berger, E., Fong, W., et al. 2017, ApJL, 848, L20
Matsumoto, T., Nakar, E., & Piran, T. 2019, MNRAS, 483, 1247
Mooley, K. P., Deller, A. T., Gottlieb, O., et al. 2018a, Natur, 561, 355
Mooley, K. P., Frail, D. A., Dobie, D., et al. 2018b, ApJL, 868, L11
Mooley, K. P., Nakar, E., Hotokezaka, K., et al. 2018c, Natur, 554, 207
Murguia-Berthier, A., Ramirez-Ruiz, E., Montes, G., et al. 2017, ApJL, 835, L34
Nagakura, H., Hotokezaka, K., Sekiguchi, Y., Shibata, M., & Ioka, K. 2014, ApJL, 784, L28
Nakar, E., Gottlieb, O., Piran, T., Kasliwal, M. M., & Hallinan, G. 2018, ApJ, 867, 18
Nynka, M., Ruan, J. J., Haggard, D., & Evans, P. A. 2018, ApJL, 862, L19
Pe'er, A. 2012, ApJL, 752, L8
Piro, L., Troja, E., Zhang, B., et al. 2019, MNRAS, 483, 1912
Resmi, L., Schulze, S., Ishwara-Chandra, C. H., et al. 2018, ApJ, 867, 57
Schlafly, E. F., & Finkbeiner, D. P. 2011, ApJ, 737, 103
STSCI Development Team 2012, DrizzlePac: HST Image Software, Astrophysics Source Code Library, ascl:1212.011
Tanvir, N. R., Levan, A. J., González-Fernández, C., et al. 2017, ApJL, 848, L27
Troja, E., Piro, L., Ryan, G., et al. 2018, MNRAS, 478, L18
Troja, E., Piro, L., van Eerten, H., et al. 2017, Natur, 551, 71
van Eerten, E. T. H., Ryan, G., Ricci, R., et al. 2018, arXiv:1808.06617
van Eerten, H., van der Horst, A., & MacFadyen, A. 2012, ApJ, 749, 44
van Eerten, H. J., & MacFadyen, A. I. 2012, ApJ, 751, 155
Xie, X., Zrake, J., & MacFadyen, A. 2018, ApJ, 863, 58
Zhang, B. B., Zhang, B., Sun, H., et al. 2018, NatCo, 9, 447